

Research Article www.acsami.org

Four-Phonon Scattering Effect and Two-Channel Thermal Transport in Two-Dimensional Paraelectric SnSe

Jie Sun, ** Cunzhi Zhang, ** Zhonghua Yang, Yiheng Shen, Ming Hu, ** and Qian Wang **



Cite This: ACS Appl. Mater. Interfaces 2022, 14, 11493-11499



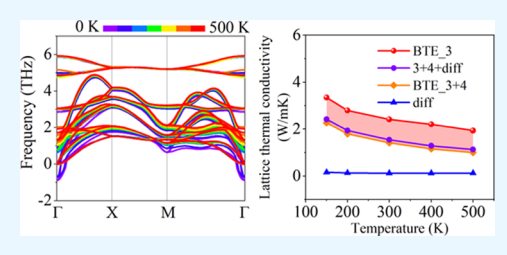
ACCESS I

Metrics & More

Article Recommendations

Supporting Information

ABSTRACT: In recent years, increased attention has been paid to the study of four-phonon interactions and diffusion transport in three-dimensional (3D) thermoelectric materials because they play an essential role in understanding the thermal transport process. In this work, we study four-phonon scattering and diffusion transport in two-dimensional (2D) thermoelectric materials using the paraelectric phase of 2D SnSe as an example. The inherent soft phonon modes are treated by the self-consistent phonon theory, which considers the temperatureinduced renormalization of the phonons. Based on density functional theory and the Peierls-Boltzmann transport equation for phonons, we show that the four-



phonon interactions can reduce the thermal conductivity of the 2D SnSe sheet by nearly 40% due to the collapse of soft optical modes, and the contribution of diffusion transport to the total thermal conductivity accounts for 14% at a high temperature of 800 K due to the short phonon mean free path approaching the Ioffe-Regel limit, suggesting the two-channel transport in this system. The results are further confirmed by using the machine learning-assisted molecular dynamics simulations. This work provides a new insight into the physical mechanisms for thermal transport in 2D systems with strong anharmonic effects.

KEYWORDS: thermal conductivity, thermoelectric materials, machine learning, two-dimensional SnSe, four-phonon scattering, two-channel transport

1. INTRODUCTION

During the past few decades, extensive theoretical studies based on the theory of phonon Boltzmann transport equation (BTE) have been carried out to calculate the thermal conductivity of materials, and the calculated results are consistent with the experimental ones to some degree. However, in recent years, it has been found that for bulk materials with some peculiar phonon dispersions such as the flatness of phonon branches, a large frequency band gap, and acoustic bunching,³ the BTE calculations including only the three-phonon scattering process fail to give an accurate prediction of their thermal conductivity. ⁴⁻⁶ A similar problem has also been found in some other materials where the threephonon phase spaces are restricted. ^{7–9} However, the difference between the theoretical and experimental results can be eliminated by taking into account the higher order fourphonon scattering.8 Although great advances in the fourphonon scattering theory have been made, a comprehensive understanding of the thermal transport properties for the materials with ultralow thermal conductivity remains challenging. First, the temperature effects on the strong anharmonicity are usually ignored in previous work. Second, for the materials with ultralow thermal conductivity where phonon mean free path (MFP) is smaller than the distance between two neighboring atoms, the BTE theory has been found to underestimate thermal conductivity as it only considers the particle-like phonon propagation. Beyond the BTE calculation,

hydrodynamics can describe the phonon Poiseuille flow and second sound, which was found in suspended graphene and silicon nanowires. 10,111 Besides, to deal with such inaccuracy, a two-channel transport theory that considers both the wave-like tunneling of phonons (diffusion transport) and particle-like propagation (nondiffusion transport) contributions to the thermal conductivity has been recently developed. It has been used successfully in studying the thermal transport properties of the systems with ultralow thermal conductivity. 12,13 For instance, based on this theory, the compound of Cu₁₂Sb₄S₁₃ was found to exhibit nearly temperature-independent and extremely low thermal conductivity, less than 1.0 W/mK, which is more consistent with the experimental results.¹⁴

However, to date, the aforementioned two-channel thermal transport mechanisms and the effect of temperature on the anharmonicity with phase transition have not been studied in 2D materials. 2D SnSe, as a typical representative of the nextgeneration electronic materials, has attracted world-wide attention because of its fantastic properties. It exhibits ferroelectricity, 15 which can be considered as the promising

Received: December 17, 2021 Accepted: February 11, 2022 Published: February 22, 2022





solution for the disappearance of the ferroelectricity when the thickness of 3D ferroelectric (FE) materials is reduced. ^{16,17} In addition, similar to its 3D counterpart, 2D SnSe possesses an ultralow thermal conductivity of 1 W/mK at 300 K and exhibits great potential in the application of thermoelectric field. ^{18–21} Therefore, understanding its thermal transport properties is of vital importance for the future application as a thermoelectric or FE material. Although many studies have been carried out on the thermal conductivity of 2D SnSe, they all are based on the three-phonon theory, resulting in the inaccuracy of the calculations, ^{22–25} and none of them consider the four-phonon scattering as well as the diffusion thermal transport.

In this work, for the first time, we systematically study the lattice thermal conductivity of 2D SnSe by taking into account the four-phonon scattering, temperature effects on the lattice anharmonicity, and its diffusion thermal transport. We show that the four-phonon scattering plays a significant role in the thermal transport process of 2D SnSe, and the diffusion phonon transport also makes an important contribution to the thermal conductivity.

2. RESULTS AND DISCUSSION

2.1. Geometric Structures. The 2D SnSe structure contains two Sn and two Se atoms in its unit cell and possesses the symmetry of Pnma at low temperatures. ¹⁵ Similar to bulk SnSe, 2D SnSe undergoes a phase transition from FE phase to paraelectric (PE) phase with the symmetry of $Pnm2_1$. ²⁶ The PE phase is semiconducting with a band gap of 0.91 eV at the PBE level, as shown in Figure S1. The lattice parameters of the FE phase along the a (armchair) and b (zigzag) directions are 4.38 and 4.29 Å, respectively. The corresponding values for the PE phase along the in-plane directions are both 4.31 Å. The top view of the PE phase is shown in Figure 1a, and the side views of the two phases are

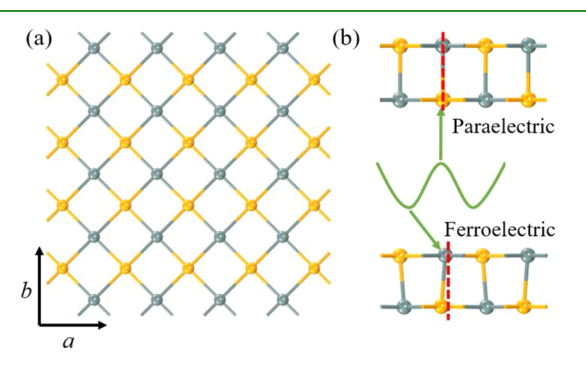


Figure 1. (a) Top view of the paraelectric phase structure. (b) Side view of the paraelectric and ferroelectric phases of 2D SnSe. The yellow and gray spheres are Se and Sn atoms, respectively. The green curve is the schematic of the W-shape potential well transition between the two phases. The red dash lines are along the out-of-plane direction.

presented in Figure 1b. One can see that the Sn—Se bonds of PE phase are parallel to the out-of-plane direction, leading to zero polarization in this structure, while for the FE phase, the Sn—Se bonds have an acute angle along the out-of-plane direction, leading to nonzero polarization in the plane. The displacement of Sn and Se atoms along the armchair direction results in a characteristic of double-well potential energy, as shown in Figure 1b. The thermal conductivity of the FE phase

of 2D SnSe has been calculated without considering the phase transition.²⁵ However, for the PE phase structures of FE materials, less theoretical studies have been conducted for the thermal transport behavior. This is because the PE phase is only stable at high temperatures and exhibits imaginary modes under the harmonic approximation, which is the commonly used method in previous calculations [0 K density functional theory (DFT)]. It prevents the precise calculation of their thermal conductivity. Very recently, Villanova et al. calculated the thermal conductivities for both the PE and FE phases of 2D SnSe using the MD simulations with the help of temperature-dependent effective potential and found that the difference in the thermal conductivities between the two phases was nontrivial.²⁷ However, the MD simulations may overlook the quantum effects when considering the interatomic forces between different atoms and cannot describe the physical process clearly. More importantly, no detailed mechanisms of phonon transport were provided in their study, such as the three-phonon vs four-phonon transport and diffusion transport behaviors.

2.2. Temperature-Dependent Phonon Dispersions. Here, with the help of self-consistent phonon (SCPH) theory, ²⁸ which considers the temperature effects to renormalize the phonons, the lattice instabilities of 2D SnSe with PE phase are treated successfully. The fourth-order force constants needed in the SCPH calculations are obtained by training the data using the Hiphive package. ^{29,30} The cutoff in the cluster space is set to 12.5 Å during the SCP calculations, and the portion of the new parameter vector is set as 0.2 to obtain the corrected harmonic model. The iteration step is set as 15 to renew the harmonic frequency under each temperature. The Monte Carlo rattle method in Hiphive is used to generate the configurations as training data. The cutoff distances for the second-, third-, and fourth-order interatomic force constant calculations are considered, and their convergence tests are conducted, as shown in Figure S2.

The temperature-dependent phonon dispersion of the PE phase in the temperature range of 0 to 500 K is shown in Figure 2a. One can see the imaginary optical branches near the

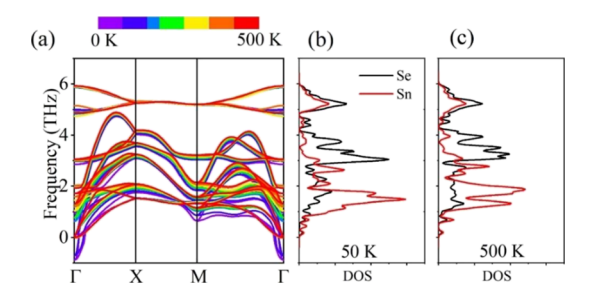


Figure 2. (a) Renormalized phonon dispersion of the PE phase of 2D SnSe at finite temperature. (b,c) Partial DOS of the PE phase at 50 and 500 K, respectively.

 Γ point at low temperature. These soft imaginary optical modes are considered as the driving mechanism of spontaneous symmetry breaking in FE materials, as is the case in other FE systems, such as the CsPbCl₃, CsSnI₃, and SrTiO₃, which possess the perovskite structures. ^{31–33} When the temperature is above the critical temperature T_c of phase transition, the frequencies of these soft modes become positive, leading to the structural transition of 2D SnSe from the low symmetry (FE phase) to the high symmetry (PE phase). By

increasing the temperature gradually, it is found that the unstable optical modes can be eliminated at 80 K, where the FE to PE phase transition occurs. Because the FE phase can exist only at the temperature below 80 K, we focus on studying the thermal transport of the PE phase of 2D SnSe because this phase can exist in a wide temperature range. We note that our calculated T_c value is smaller than that experimentally obtained³⁴ because 2D SnSe usually has interactions with the substrate in the experiment, while the structure used for our calculations is in the free-standing state. From Figure 2a, one can see that the frequencies of acoustic branches are hardening with the temperature, and a slight increase is observed in some optical branches, which can affect the thermal conductivity effectively by increasing the phonon group velocities. Figure 2b,c shows the partial density of states (PDOS) of the Se and Sn atoms at the low temperature (50 K) and high temperature (500 K), respectively. In the low frequency region (0-2 THz), the PDOS of the Sn atoms has a red shift trend, leading to the increased phonon group velocities. In the high frequency region (2-5 THz), the temperature effects are mainly contributed by the Se atoms.

2.3. Thermal Transport Properties. The materials with low thermal conductivities usually exhibit large anharmonicity, which can be directly reflected by the scattering rates. The importance of four-phonon scatterings has been demonstrated in some bulk materials with high thermal conductivity.^{3,7,38} Only a very recent work reported the four-phonon scatterings in the monolayer MoO3, which exhibits an ultralow thermal conductivity.³⁶ Here, we also consider the three- and fourphonon interactions in the 2D SnSe sheet. A q-point mesh of $20 \times 20 \times 1$ is used for the calculation, which is equivalent to the supercells employed in the following MD simulations. The thickness is set as 9.5 Å. The detailed information can be found in Section 4 in the Supporting Information. The Dirac delta function is regularized by the Gaussian function.³⁷ The width parameter for the scattering processes is obtained by setting the scalebroad to 1.0 and fixed to 0.01 rad/ps for the fourphonon scattering process. The convergence of the scalebroad and the width parameter are presented in Figure S3.

Figure 3a,b shows the calculated scattering rates considering the three- and four-phonon interactions separately at the temperatures of 300 and 500 K, respectively. The four-phonon scattering rates are quite strong and comparable to those of three-phonon scattering processes whether at low or high temperatures. Besides, at 500 K, the occupation of fourphonon scattering rates becomes more important as compared to that of 300 K. More specifically, at 300 K, the four-phonon scattering rates are slightly smaller than those of three-phonon scattering rates in the frequency range of 0-3 THz. When the temperature reaches 500 K, the four-phonon scattering rates nearly get overlapped with and even become larger than the three-phonon scattering rates. It is also found that the scattering rates for both three- and four-phonon interactions increase with temperature, which indicates a lower thermal conductivity at higher temperatures.

To validate the BTE results, we also calculate the scattering rates by using MD simulations from another perspective. The interatomic potentials describing the atomic forces on the Sn and Se atoms are trained with the deep neural network using the DeepMD package. The detailed information can be obtained in Section 6 in the Supporting Information. To verify the accuracy of the DeepMD potential, we compare the calculated forces on each atom by using DFT and DeepMD

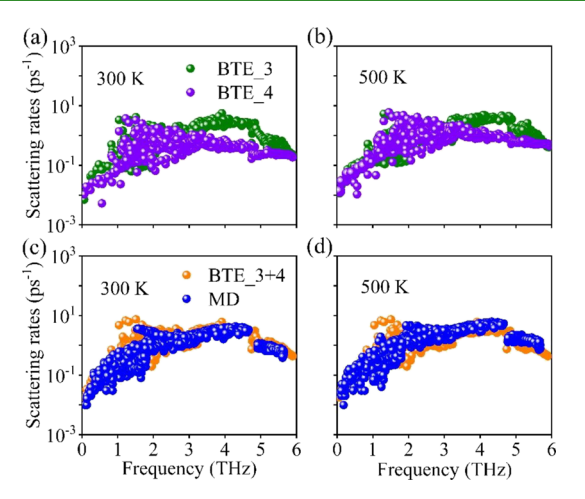


Figure 3. Phonon scattering rate of 2D SnSe considering three- and four-phonon interactions separately at temperature of (a) 300 K and (b) 500 K. Scattering rate obtained from BTE calculations considering both three- and four-phonon interactions and from MD simulations at temperature of (c) 300 K and (d) 500 K.

potential. Based on the second-, third-, and fourth-order force constants, the phonon group velocity and scattering rates based on BTE method at 300 K are calculated and compared as shown in Figure S4. After verifying the accuracy of DeepMD potential, the calculated scattering rates via MD simulations are shown in Figure 3c,d, which are extracted from the MD trajectories for 1 ns and 400 ps simulations at 300 and 500 K, respectively, using the spectral energy density (SED) methods as implemented in the Dynaphopy package. 40 The size of the supercell during the simulation is set to $20 \times 20 \times 1$, and the temperature-dependent second-order force constants are used to calculate the scattering rates in our SED calculations. We choose a simulation time of 400 ps for temperature at 500 K, which is enough to extract the phonon lifetime due to the stronger phonon scattering at a higher temperature. One can see that the obtained total scattering rates including both three- and four-phonon interactions are consistent with the results of the MD simulations, showing the validity of our calculated three- and four-phonon scattering rates. The advantage of the BTE calculations is that one can see the contributions of the two parts clearly.

Because most previous calculations of the thermal conductivities only consider the three-phonon scattering processes, it is of importance to identify the characteristic of those materials, where the four-phonon scatterings may play important roles. It is well-known that the phonon properties and thermal conductivity are mainly determined by the anharmonicity of the structure, which can also be depicted by the potential energy profile. The most widely used method to calculate the potential energy is by adding volumedependent vibrational free energy, while it is not applicable to the materials with unstable phonon modes. Another approach is to guess the unstable directions by using the phonon eigenvectors obtained with DFT calculations. Here, by using the frozen phonon-perturbed theory,⁴¹ the total energies for the soft optical mode at Γ point are calculated. A displacement is imposed on each atom in the primitive cell as follows

$$u(\eta) = \eta \cdot e(q_{\Gamma} \nu) \tag{1}$$

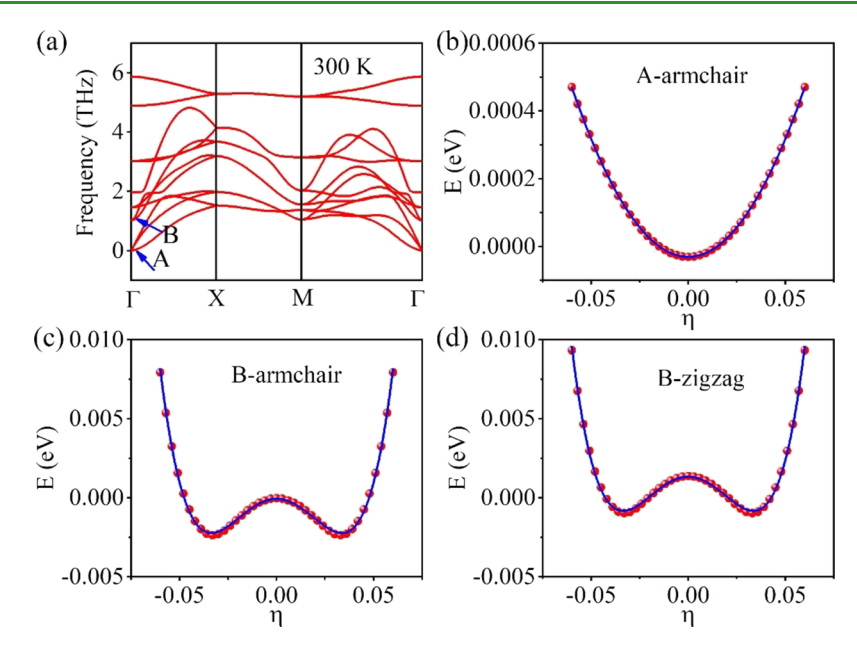


Figure 4. (a) Phonon dispersion of 2D SnSe at 300 K calculated by the SCPH theory. Potential curve of the vibrational modes in 2D SnSe (b) for mode A along the armchair direction and (c)/(d) for mode B along the armchair/zigzag direction.

where η is the scaling factor and e is the chosen soft mode eigenvector obtained from the phonon calculations. According to the Laudau theory and the adiabatic approximation, ⁴² the electronic system changes instantaneously after new ionic positions are reached. The anharmonic energy as a function of displacement can be expressed by

$$U(\eta) = U_0 + \frac{u^2}{4}\hbar\omega(q_{\Gamma}\nu) + \frac{u^4}{24}\Phi_4 + O(u^6)$$
 (2)

where U is the total anharmonic energy, U_0 is the anharmonic energy at the equilibrium state, u is the displacement, ω is the frequency of phonon mode q at the Γ point, ν is the mode label, Φ_4 is the anharmonic energy to the fourth order, and O represents the higher order of anharmonic energy.

We choose the phonon dispersion of the structure at 300 K as an example. The results are shown in Figure 4. Two phonon modes near the Γ point, labeled as "A" and "B" in Figure 4a, are chosen to calculate the potential energy. As seen in Figure 4b, the potential energy profile of the acoustic mode A (ZA with frequency 0.065 THz) shows a perfect parabolic characteristic. In contrast, as clearly seen from Figure 4c,d, the energy profiles of the mode B fit very well with fourthorder model, exhibiting a signature of strong four-phonon scatterings for atoms moving in both armchair and zigzag directions. The mode B is actually a soft optical mode, which exhibits negative frequency at low temperatures. When the temperature is above the T_c , the frequencies of these soft optical phonon modes become positive, leading to the phonon collapse. The strong anharmonicity and the fourth-order potential curves of the soft optical mode are a general characteristic in the FE materials. In addition, it is noted that the mode B is at the frequency of 1 THz, showing that fourphonon scattering can be important around this frequency region. This is consistent with the calculated scattering rates shown in Figure 3, where the four-phonon scattering rates can reach the highest value around 1 THz. The strong anharmonic effects existing in the FE materials with soft optical modes are

demonstrated by the calculations of four-phonon scattering rate in this work.

Based on the stabilized phonon dispersions and scattering rates, we then calculate the lattice thermal conductivity of 2D SnSe with the PE phase. The results of the thermal conductivity at different levels of phonon transport mechanisms are shown in Figure 5a. By only considering the three-

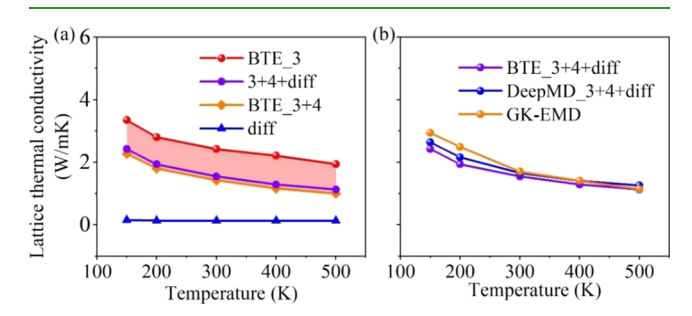


Figure 5. (a) Lattice thermal conductivity of 2D SnSe calculated at different levels of phonon transport mechanisms. (b) Comparison of the thermal conductivity between the DFT-based BTE method and the machine learning potential-based classical GK-EMD simulations.

phonon scattering process, the lattice thermal conductivities of 2D SnSe are 3.47, 2.96, 2.42, 2.22, and 2.06 W/mK at the temperatures of 150, 200, 300, 400, and 500 K, respectively. It is found that the thermal conductivities decrease as the temperature increases, which results from the higher scattering rates at higher temperatures, as seen in Figure 3. When taking four-phonon scattering into consideration, the corresponding thermal conductivities are reduced to 2.35, 1.89, 1.43, 1.25, and 1.08 W/mK, showing the significant effect (negative) of the four-phonon scattering. Especially, the thermal conductivity at 300 K is decreased by as large as 40% when the fourphonon interactions are considered. The scattering process including four-phonon interactions can allow for more phonon scattering channels, which is forbidden under the condition of three-phonon scattering, leading to a large reduction in the total thermal conductivity.

On the other hand, when the phonon MFP reaches the length on the order of interatomic distances, known as the Ioffe–Regel limit, ⁴³ the thermal transport will show the diffusion behavior, a common phenomenon in the disordered materials. ^{44,45} Hanus et al. also defined the off-diagonal component of the heat-flux operator as a diffusion channel for the thermal transport. ⁴⁶ Then, the total thermal conductivity of a crystal reads

$$\kappa_{\text{tot}} = \kappa_{\text{ph}} + \kappa_{\text{diff}}$$
(3)

01

$$\kappa^{\alpha\beta} = \kappa_{p}^{\alpha\beta} + \frac{\hbar^{2}}{k_{B}T^{2}} \frac{1}{VN_{c}} \sum_{q} \sum_{s \neq s'} \frac{\omega(q)_{s} + \omega(q)_{s'}}{2} v^{\alpha}(q)_{s,s'} v^{\beta}(q)_{s,s'} \times \frac{\omega(q)_{s} \overline{N}(q)_{s} (\overline{N}(q)_{s} + 1) + \omega(q)_{s'} \overline{N}(q)_{s'} (\overline{N}(q)_{s'} + 1)}{4(\omega(q)_{s} - \omega(q)_{s'})^{2} + (\Gamma(q)_{s} + \Gamma(q)_{s'})^{2}} \times (\Gamma(q)_{s} + \Gamma(q)_{s'})$$
(4)

where $\kappa_{\rm p}^{\alpha\beta}$ is the Peierls contribution to the conductivity, \hbar , $k_{\rm B}$, T, V, and $N_{\rm c}$ are the reduced Plank constant, Boltzmann constant, the absolute temperature, the unit cell volume, and number of phonon wave vectors, respectively. $v(q)_{\rm s,\ s'}$ and $\Gamma(q)_{\rm s}$ are the phonon group velocity and phonon line-width indexed by wave vector q with the branch s, respectively. The $\overline{N}(q)_{\rm s}$ is the equilibrium Bose–Einstein distribution. Eq 4 is derived from the Wigner phase-space formulation of quantum mechanics, which elucidates how the interplay between disorder, anharmonicity, and the quantum Bose–Einstein statistics of atomic vibrations determines thermal conductivity.

However, the phenomenon of the diffusion transport in 2D materials remains unexplored. We first calculate the MFP of the 2D SnSe, and the results are shown in Figure S5. The nearest neighboring atom in 2D SnSe is about 3 Å, considering the finite displacement of the atoms during the heat transfer. We note that a large portion of the MFPs is smaller than the atomic distances, indicating a nontrivial diffusion transport behavior. We then calculate the contribution to thermal conductivity from the diffusion channel; the diffusion thermal conductivities of 2D SnSe are 0.105, 0.105, 0.109, 0.116, and 0.117 W/mK at the temperatures of 150, 200, 300, 400, and 500 K, respectively. The results are shown in Figure 5a. It is found that the diffusion transport is not very sensitive to the temperature. However, because the nondiffusion thermal conductivity decreases with the temperature, the contribution of the diffusion transport becomes more important as the temperature increases. To see the occupation of diffusion transport at higher temperatures, the thermal conductivities from the diffusion and nondiffusion channel are calculated to be 0.13 and 0.82 W/mK at 800 K, respectively. We also plot the spectral lattice thermal conductivity of the diffusion transport with respect to phonon frequency up to 800 K, as shown in Figure S6, which shows the feature of diffusion transport more clearly, as demonstrated in previous work. 14,47 It is exciting to observe that the diffusion thermal conductivity can be as large as 15% of the nondiffusion thermal conductivity, which is usually neglected in other work in the 2D systems. The eventual thermal conductivity of 2D SnSe, including the three- and four-phonon scattering processes and diffusion transport, is 1.43 W/mK at 300 K, which shows a large difference from the original value of 2.42 W/mK by only considering the three-phonon scattering processes.

For comparison, we also perform classical Green-Kubo equilibrium molecular dynamics (GK-EMD) simulations to calculate the thermal conductivity. The results are shown in Figure 5b, where all orders of phonon scattering processes are included. Moreover, the size convergence of GK-EMD simulations is also checked. The calculated thermal conductivities using GK-EMD simulation with the $20 \times 20 \times 1$ supercell are 2.94, 2.49, 1.70, 1.41, and 1.14 W/mK at the temperatures of 150, 200, 300, 400, and 500 K, respectively. These are consistent with the results of the BTE method combined with the diffusion model, indicating that the hydrodynamic transport, as mentioned before, would not be important in the 2D SnSe with PE phase. However, these values are slightly higher than BTE results, particularly at low temperatures. The deviation of the results of the two methods may arise from the ignorance of the quantum effects in the phonon scattering in classical MD simulations. We notice the thermal conductivity of the 2D single-crystalline SnSe here is extremely low, that is, ~1.5 W/mK at room temperature; therefore, it can be anticipated that the grain boundaries existing in the experiment can further decrease the thermal conductivity, like in other 2D materials. 48-50

3. CONCLUSIONS

In summary, the lattice thermal transport of 2D PE SnSe is investigated and compared by using two different approaches: phonon BTE combined with first-principles calculations and the classical GK-EMD simulation with interatomic potential trained by the high fidelity deep neural network, where the anharmonic interactions up to the fourth order is considered in BTE calculations. Our results show that (1) the thermal transport of the 2D SnSe in the PE phase can only be correctly examined by the SCPH theory because pure harmonic calculation based on 0 K DFT would yield unrealistic imaginary phonon frequencies due to the inherent soft phonon modes, and the abnormal phonon hardening effect is observed at elevated temperatures; (2) four-phonon scattering is found to contribute significantly to the overall thermal transport in 2D PE SnSe (over 40% reduction to three-phonon process at room temperature); (3) the diffusion thermal transport in 2D SnSe with the PE phase is also nontrivial, leading to the twochannel thermal transport mechanism. We further conclude that the four-phonon scattering and diffusion transport should be considered in 2D materials that can exhibit the fourth-order energy profile with an MFP below the Ioffe-Regel limit. We believe that our work will inspire the exploration of a new phenomenon in the thermal transport of 2D materials and provide the basics for their future applications.

ASSOCIATED CONTENT

Supporting Information

The Supporting Information is available free of charge at https://pubs.acs.org/doi/10.1021/acsami.1c24488.

Detailed information of the settings in the density functional theory calculations; electronic property of 2D SnSe with the paraelectric phase; details of the force constant calculations; detailed information of the calculations in three- and four-phonon scattering rates; convergence test for the scalebroad and width; detailed information of the settings in obtaining the DeepMD potential; phonon mean free path of 2D SnSe with the

paraelectric phase; and the lattice thermal conductivity of diffusion transport (PDF)

AUTHOR INFORMATION

Corresponding Authors

Ming Hu — Department of Mechanical Engineering, University of South Carolina, Columbia, South Carolina 29208, United States; orcid.org/0000-0002-8209-0139; Email: hu@scedu

Qian Wang — School of Materials Science and Engineering, CAPT, HEDPS, BKL-MEMD, Peking University, Beijing 100871, China; orcid.org/0000-0002-9766-4617; Email: qianwang2@pku.edu.cn

Authors

Jie Sun – School of Materials Science and Engineering, CAPT, HEDPS, BKL-MEMD, Peking University, Beijing 100871, China

Cunzhi Zhang — Pritzker School of Molecular Engineering, University of Chicago, Chicago, Illinois 60637, United States

Zhonghua Yang — Department of Mechanical Engineering, University of South Carolina, Columbia, South Carolina 29208, United States; College of Architecture and Civil Engineering, Shenyang University of Technology, Shenyang 110870, China

Yiheng Shen — School of Materials Science and Engineering, CAPT, HEDPS, BKL-MEMD, Peking University, Beijing 100871, China

Complete contact information is available at: https://pubs.acs.org/10.1021/acsami.1c24488

Author Contributions

[#]J.S. and C.Z. made the equal contributions to this paper.

Notes

The authors declare no competing financial interest.

ACKNOWLEDGMENTS

This work is partially supported by grants from the National Key Research and Development Program of the Ministry of Science and technology of China (Grant No. 2017YFA0205003) and the National Natural Science Foundation of China (Grants Nos. NSFC-11974028 and NSFC-21773004). It is also supported by the High-Performance Computing Platform of Peking University, China. Research reported in this publication was supported in part by the NSF (award number 2030128).

REFERENCES

- (1) Xie, L.; Feng, J.; Li, R.; He, J. First-Principles Study of Anharmonic Lattice Dynamics in Low Thermal Conductivity AgCrSe₂: Evidence for a Large Resonant Four-Phonon Scattering. *Phys. Rev. Lett.* **2020**, *125*, No. 245901.
- (2) Ravichandran, N. K.; Broido, D. Phonon-Phonon Interactions in Strongly Bonded Solids: Selection Rules and Higher-Order Processes. *Phys. Rev. X* **2020**, *10*, No. 021063.
- (3) Yang, X.; Feng, T.; Li, J.; Ruan, X. Stronger role of four-phonon scattering than three-phonon scattering in thermal conductivity of III-V semiconductors at room temperature. *Phys. Rev. B* **2019**, *100*, No. 245203.
- (4) Kang, J. S.; Li, M.; Wu, H.; Nguyen, H.; Hu, Y. Experimental observation of high thermal conductivity in boron arsenide. *Science* **2018**, *361*, *575*–*578*.

- (5) Li, S.; Zheng, Q.; Lv, Y.; Liu, X.; Wang, X.; Huang, P. Y.; Cahill, D. G.; Lv, B. High thermal conductivity in cubic boron arsenide crystals. *Science* **2018**, *361*, 579–581.
- (6) Tian, F.; Song, B.; Chen, X.; Ravichandran, N. K.; Lv, Y.; Chen, K.; Sullivan, S.; Kim, J.; Zhou, Y.; Liu, T.-H. Unusual high thermal conductivity in boron arsenide bulk crystals. *Science* **2018**, *361*, 582–585
- (7) Feng, T.; Ruan, X. Four-phonon scattering reduces intrinsic thermal conductivity of graphene and the contributions from flexural phonons. *Phys. Rev. B* **2018**, *97*, No. 045202.
- (8) Feng, T.; Ruan, X. Quantum mechanical prediction of four-phonon scattering rates and reduced thermal conductivity of solids. *Phys. Rev. B* **2016**, 93, No. 045202.
- (9) Kundu, A.; Yang, X.; Ma, J.; Feng, T.; Carrete, J.; Ruan, X.; Madsen, G. K.; Li, W. Ultrahigh thermal conductivity of θ -phase tantalum nitride. *Phys. Rev. Lett.* **2021**, *126*, No. 115901.
- (10) Lee, S.; Broido, D.; Esfarjani, K.; Chen, G. Hydrodynamic phonon transport in suspended graphene. *Nat. Commun.* **2015**, *6*, 1–10
- (11) Zhou, Y.; Zhang, X.; Hu, M. Nonmonotonic diameter dependence of thermal conductivity of extremely thin Si nanowires: competition between hydrodynamic phonon flow and boundary scattering. *Nano Lett.* **2017**, *17*, 1269–1276.
- (12) Isaeva, L.; Barbalinardo, G.; Donadio, D.; Baroni, S. Modeling heat transport in crystals and glasses from a unified lattice-dynamical approach. *Nat. Commun.* **2019**, *10*, 1–6.
- (13) Simoncelli, M.; Marzari, N.; Mauri, F. Unified theory of thermal transport in crystals and glasses. *Nat. Phys.* **2019**, *15*, 809–813.
- (14) Xia, Y.; Ozolinš, V., Wolverton, C. Microscopic Mechanisms of Glasslike Lattice Thermal Transport in Cubic Cu₁₂Sb₄S₁₃ Tetrahedrites. *Phys. Rev. Lett.* **2020**, *125*, No. 085901.
- (15) Fei, R.; Kang, W.; Yang, L. Ferroelectricity and phase transitions in monolayer group-IV monochalcogenides. *Phys. Rev. Lett.* **2016**, *117*, No. 097601.
- (16) Chang, K.; Liu, J.; Lin, H.; Wang, N.; Zhao, K.; Zhang, A.; Jin, F.; Zhong, Y.; Hu, X.; Duan, W. Discovery of robust in-plane ferroelectricity in atomic-thick SnTe. *Science* **2016**, *353*, 274–278.
- (17) Liu, K.; Lu, J.; Picozzi, S.; Bellaiche, L.; Xiang, H. Intrinsic origin of enhancement of ferroelectricity in SnTe ultrathin films. *Phys. Rev. Lett.* **2018**, *121*, No. 027601.
- (18) Chandra, S.; Biswas, K. Realization of high thermoelectric figure of merit in solution synthesized 2D SnSe nanoplates via Ge alloying. *J. Am. Chem. Soc.* **2019**, *141*, 6141–6145.
- (19) Chandra, S.; Dutta, P.; Biswas, K. Enhancement of the Thermoelectric Performance of 2D SnSe Nanoplates through Incorporation of Magnetic Nanoprecipitates. *ACS Appl. Energy Mater.* **2020**, *3*, 9051–9057.
- (20) Zhou, Y.; Zhao, L. D. Promising thermoelectric bulk materials with 2D structures. *Adv. Mater.* **2017**, *29*, No. 1702676.
- (21) Heo, S. H.; Jo, S.; Kim, H. S.; Choi, G.; Song, J. Y.; Kang, J.-Y.; Park, N.-J.; Ban, H. W.; Kim, F.; Jeong, H. Composition changedriven texturing and doping in solution-processed SnSe thermoelectric thin films. *Nat. Commun.* **2019**, *10*, 1–10.
- (22) Nag, S.; Saini, A.; Singh, R.; Kumar, R. Ultralow lattice thermal conductivity and anisotropic thermoelectric performance of AA stacked SnSe bilayer. *Appl. Surf. Sci.* **2020**, *512*, No. 145640.
- (23) Sun, Y.; Shuai, Z.; Wang, D. Reducing Lattice Thermal Conductivity of the Thermoelectric SnSe Monolayer: Role of Phonon–Electron Coupling. *J. Phys. Chem. C* **2019**, *123*, 12001–12006
- (24) Hu, Z.-Y.; Li, K.-Y.; Lu, Y.; Huang, Y.; Shao, X.-H. High thermoelectric performances of monolayer SnSe allotropes. *Nanoscale* **2017**, *9*, 16093–16100.
- (25) Wang, F. Q.; Zhang, S.; Yu, J.; Wang, Q. Thermoelectric properties of single-layered SnSe sheet. *Nanoscale* **2015**, *7*, 15962–15970
- (26) Zhao, L.-D.; Lo, S.-H.; Zhang, Y.; Sun, H.; Tan, G.; Uher, C.; Wolverton, C.; Dravid, V. P.; Kanatzidis, M. G. Ultralow thermal

- conductivity and high thermoelectric figure of merit in SnSe crystals. *Nature* **2014**, *508*, 373–377.
- (27) Villanova, J. W.; Barraza-Lopez, S. Anomalous thermoelectricity at the two-dimensional structural transition of SnSe monolayers. *Phys. Rev. B* **2021**, *103*, No. 035421.
- (28) Errea, I.; Calandra, M.; Mauri, F. Anharmonic free energies and phonon dispersions from the stochastic self-consistent harmonic approximation: Application to platinum and palladium hydrides. *Phys. Rev. B* **2014**, *89*, No. 064302.
- (29) Eriksson, F.; Fransson, E.; Erhart, P. The Hiphive Package for the Extraction of High-Order Force Constants by Machine Learning. *Adv. Theory Simul.* **2019**, *2*, No. 1800184.
- (30) Fransson, E.; Eriksson, F.; Erhart, P. Efficient construction of linear models in materials modeling and applications to force constant expansions. *npj Comput. Mater.* **2020**, *6*, 1–11.
- (31) Fujii, Y.; Hoshino, S.; Yamada, Y.; Shirane, G. Neutron-scattering study on phase transitions of CsPbCl₃. *Phys. Rev. B* **1974**, *9*, 4540
- (32) Patrick, C. E.; Jacobsen, K. W.; Thygesen, K. S. Anharmonic stabilization and band gap renormalization in the perovskite CsSnI₃. *Phys. Rev. B* **2015**, 92, No. 201205.
- (33) Tadano, T.; Tsuneyuki, S. Self-consistent phonon calculations of lattice dynamical properties in cubic SrTiO 3 with first-principles anharmonic force constants. *Phys. Rev. B* **2015**, *92*, No. 054301.
- (34) Chang, K.; Küster, F.; Miller, B. J.; Ji, J.-R.; Zhang, J.-L.; Sessi, P.; Barraza-Lopez, S.; Parkin, S. S. Microscopic manipulation of ferroelectric domains in SnSe monolayers at room temperature. *Nano Lett.* **2020**, *20*, 6590–6597.
- (35) Feng, T.; Lindsay, L.; Ruan, X. Four-phonon scattering significantly reduces intrinsic thermal conductivity of solids. *Phys. Rev. B* **2017**, *96*, No. 161201.
- (36) Tong, Z.; Dumitrică, T.; Frauenheim, T. Ultralow Thermal Conductivity in Two-Dimensional MoO₃. *Nano Lett.* **2021**, 21, 4351–4356.
- (37) Li, W.; Carrete, J.; Katcho, A.; Mingo, N. ShengBTE: A solver of the Boltzmann transport equation for phonons. *Comput. Phys. Commun.* **2014**, *185*, 1747–1758.
- (38) Rodriguez, A.; Liu, Y.; Hu, M. Spatial density neural network force fields with first-principles level accuracy and application to thermal transport. *Phys. Rev. B* **2020**, *102*, No. 035203.
- (39) Wang, H.; Zhang, L.; Han, J.; Weinan, E. DeePMD-kit: A deep learning package for many-body potential energy representation and molecular dynamics. *Comput. Phys. Commun.* **2018**, 228, 178–184.
- (40) Carreras, A.; Togo, A.; Tanaka, I. DynaPhoPy: A code for extracting phonon quasiparticles from molecular dynamics simulations. *Comput. Phys. Commun.* **2017**, *221*, 221–234.
- (41) Marronnier, A.; Lee, H.; Geffroy, B.; Even, J.; Bonnassieux, Y.; Roma, G. Structural instabilities related to highly anharmonic phonons in halide perovskites. *J. Phys. Chem. Lett.* **2017**, *8*, 2659–2665.
- (42) Cowley, R. Structural phase transitions I. Landau theory. *Adv. Phys.* **1980**, 29, 1–110.
- (43) Mukhopadhyay, S.; Parker, D. S.; Sales, B. C.; Puretzky, A. A.; McGuire, M. A.; Lindsay, L. Two-channel model for ultralow thermal conductivity of crystalline Tl3VSe4. *Science* **2018**, *360*, 1455–1458.
- (44) Jain, A. Multichannel thermal transport in crystalline Tl3VSe4. *Phys. Rev. B* **2020**, *102*, No. 201201.
- (45) Pal, K.; Xia, Y.; Wolverton, C. Microscopic mechanism of unusual lattice thermal transport in TlInTe 2. *npj Comput. Mater.* **2021**, 7, 1–8.
- (46) Hanus, R.; George, J.; Wood, M.; Bonkowski, A.; Cheng, Y.; Abernathy, D. L.; Manley, M. E.; Hautier, G.; Snyder, G. J.; Hermann, R. P. Uncovering design principles for amorphous-like heat conduction using two-channel lattice dynamics. *Mater. Today Phys.* **2021**, *18*, No. 100344.
- (47) Zeng, Z.; Zhang, C.; Yu, H.; Li, W.; Pei, Y.; Chen, Y. Ultralow and glass-like lattice thermal conductivity in crystalline BaAg₂Te₂: Strong fourth-order anharmonicity and crucial diffusive thermal transport. *Mater. Today Phys.* **2021**, 21, No. 100487.

- (48) Gao, Y.; Zhou, Y.; Zhang, X.; Hu, M. Extremely low thermal conductivity of polycrystalline silicene. *J. Phys. Chem. C* **2018**, *122*, 9220–9228.
- (49) Sun, J.; Guo, Y.; Wang, Q.; Kawazoe, Y. Thermal transport properties of penta-graphene with grain boundaries. *Carbon* **2019**, 145, 445–451.
- (50) Liu, H.; Lin, Y.; Luo, S. Grain boundary energy and grain size dependences of thermal conductivity of polycrystalline graphene. *J. Phys. Chem. C* **2014**, *118*, 24797–24802.

